Applied Physics Letters

An accurate locally active memristor model for S-type negative differential resistance in NbO_x

Cite as: Appl. Phys. Lett. **108**, 023505 (2016); https://doi.org/10.1063/1.4939913
Submitted: 28 October 2015 • Accepted: 03 January 2016 • Published Online: 14 January 2016

Gary A. Gibson, Srinitya Musunuru, Jiaming Zhang, et al.

AIP Publishing

An accurate locally active memristor model for S-type negative differential resistance in NbO_x

Gary A. Gibson,[1] Srinitya Musunuru,[1] Jiaming Zhang,[1] Ken Vandenberghe,[2] James Lee,[1] Cheng-Chih Hsieh,[1] Warren Jackson,[1] Yoocharn Jeon,[1] Dick Henze,[1] Zhiyong Li,[1] and R. Stanley Williams[1]
[1]*Hewlett-Packard Laboratories, 1501 Page Mill Road, Palo Alto, California 94304, USA*
[2]*PTD-PPS, Hewlett-Packard Company, 1070 NE Circle Boulevard, Corvallis, Oregon 97330, USA*

(Received 28 October 2015; accepted 3 January 2016; published online 14 January 2016)

A number of important commercial applications would benefit from the introduction of easily manufactured devices that exhibit current-controlled, or "S-type," negative differential resistance (NDR). A leading example is emerging non-volatile memory based on crossbar array architectures. Due to the inherently linear current vs. voltage characteristics of candidate non-volatile memristor memory elements, individual memory cells in these crossbar arrays can be addressed only if a highly non-linear circuit element, termed a "selector," is incorporated in the cell. Selectors based on a layer of niobium oxide sandwiched between two electrodes have been investigated by a number of groups because the NDR they exhibit provides a promisingly large non-linearity. We have developed a highly accurate compact dynamical model for their electrical conduction that shows that the NDR in these devices results from a thermal feedback mechanism. A series of electrothermal measurements and numerical simulations corroborate this model. These results reveal that the leakage currents can be minimized by thermally isolating the selector or by incorporating materials with larger activation energies for electron motion.
[http://dx.doi.org/10.1063/1.4939913]

Devices exhibiting negative differential resistance (NDR) can be classified into two categories: current-controlled (CC-NDR), or S-type, and voltage-controlled (VC-NDR), or N-type. Circuit elements exhibiting N-type NDR are available in the form of Esaki diodes,[1,2] Gunn diodes, impact ionization avalanche transit time (or IMPATT) diodes, tunnel injection transit time or TUNNETT diodes, and resonant tunnel diodes (RTD). On the other hand, although S-type NDR has been observed in structures exhibiting interband tunneling,[3,4] threshold switching,[5–7] electronic instabilities,[8,9] insulator-metal transitions in metal oxides,[10–20] and as a precursor to memristive on-switching,[21–23] S-type discrete or integrated circuit components are not readily available.

The advent of easily fabricated S-type NDR devices would be of great commercial interest both as a circuit element in existing technologies and as an enabler of emerging technologies. A prime example of the latter is resistance-based memory technologies that utilize memristive, phase-change, conductive bridge, or spin-torque memory elements[24] in crossbar array architectures. These technologies are under intense development due to their potential for providing fast, low-power, non-volatile random-access memory (NV-RAM). Such memory would revolutionize computer architectures by facilitating the consolidation of memory and storage, ultimately replacing hard drives, Flash, and conventional DRAM in both memory and storage roles. One of the prime impediments to utilization of these emerging NV-RAM technologies is that they store information in the form of resistances that depend only weakly on voltage. Consequently, when used in crossbar arrays, these memory elements must be paired with a highly non-linear two-terminal circuit element that passes current when the full voltage is applied across an addressed memory cell but sharply limits the current leaking through partially biased memory cells in the array.[25] Without such a "selector," reading and writing individual linear memory elements in a large array are not possible. The extremely non-linear current-voltage characteristics of NDR devices are ideal for this role. Note that conventional diode technologies do not meet all the requirements of a selector, which include small size, low temperature CMOS-compatible back-end-of-line manufacture, high current density operation, and, in most cases, *bipolar operation*. We describe here an easily manufactured, bipolar, room temperature S-type NDR circuit element that fulfills the needs of a crossbar memory selector. These devices rely on the fact that any electrical conduction mechanism whose conductivity depends strongly enough on temperature can, in principle, exhibit NDR due to Joule self-heating at sufficiently large biases and currents.[26] In practice, NDR is only observed for a limited set of conduction mechanisms where the onset of NDR occurs at temperatures and fields low enough for the device's materials to survive. This paper is focused on an instantiation of a Joule-heating based S-type NDR selector based on niobium oxide (NbO_x).

Figure 1 shows a cross-sectional transmission electron microscope (TEM) image of one of these selectors. To create these devices, planarized substrates were prepared that included TiN nanovias through a dielectric bilayer of SiO_2 and Si_3N_4. These nanovias range from 32 nm to 2 μm across and are connected at the bottom to a common tungsten electrode. Blanket films of NbO_x, TiN, Pt, and Cr were deposited on top of these substrates after removing the native oxide from the exposed surface of the TiN nanovias. The NbO_x

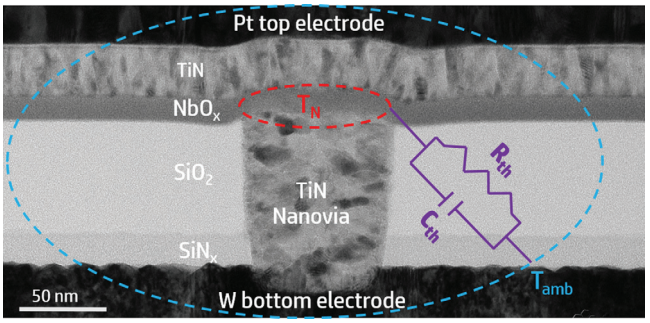

FIG. 1. Bright field cross-sectional TEM image of representative NbO_x selector. Active area of NbO_x is assumed to be at a uniform temperature T_N that is higher than the surrounding ambient temperature, T_{amb}, due to Joule heating. This heated region is thermally connected to T_{amb} through the effective thermal resistance, R_{th}, and thermal capacitance, C_{th}, of the surrounding device structures.

was created by reactively sputtering Nb in different partial pressures of oxygen to create samples with values of x near either 2 or 2.5 as determined from x-ray photoelectron spectroscopy measurements. TEM-based electron diffraction shows that the NbO_x films were amorphous as deposited. The Cr was included as a hard etch mask for photolithographically patterning top Pt contacts above each nanovia, which enabled individual testing of the resulting isolated selectors.

After an initial electrical forming process, stable NDR is observed in the devices with starting Nb to O ratios near 2:5 ("a-Nb_2O_5"), but not in those that start with a 1:2 ratio ("a-NbO_2"). The initially oxygen rich samples are formed by applying slow (~1 s) logarithmic current ramps with successively greater amplitude using a Keysight B1500 Parameter Analyzer. Depending upon the a-Nb_2O_5 layer thickness, the forming proceeds in one of two ways. For thinner devices, the conductivity increases and a region of NDR appears in their voltage vs. current characteristics (V-I) at higher currents (type I forming). The conductivity of thicker devices also increases initially but then abruptly decreases, again resulting in NDR at higher currents (type II forming, see supplementary Figure S1 for representative progression of V-I curves for both forming types).[50] In both cases, the process is stopped when increasing the amplitude of the current sweep no longer changes the V-I curves. The sweep currents required to reach a stable state and the resulting low bias conductance both scale with the area of the bottom contact for both types of forming, suggesting that the entire region above the contact is formed. The nature of these forming processes will be described in detail in a future publication. Briefly, TEM-based electron energy-loss spectroscopy composition maps and electron diffraction measurements on cross-sections of the formed selectors reveal that the a-Nb_2O_5 is reduced by reaction with the TiN electrodes during both type I and type II forming processes. For type II devices, this reduction is followed by crystallization into the tetragonal NbO_2 structure, which impedes further reduction. Films with a starting composition near a-NbO_2 on the other hand are rapidly reduced, before crystallization can occur, to a composition that is too close to metallic to exhibit NDR. Empirically, selectors with the thickest tested a-Nb_2O_5 layers (42 nm) usually underwent type II forming, although a metastable type I state could sometimes be achieved through careful control of the maximum applied current. Stabilizing a partially reduced type I state became easier for thinner films, with the thinnest tested layers (8 nm) always exhibiting only type I forming (see supplementary material for further discussion of the electrical forming process).[50]

A number of groups have investigated the strong NDR exhibited by NbO_2 layers sandwiched between two, typically Pt, electrodes.[27–32] This NDR is frequently attributed to the insulator-metal transition (IMT) that occurs at 1080 K in crystalline NbO_2.[33] However, we observe NDR in NbO_x films that are amorphous and have Nb to O ratios other than 1:2. The NDR in these devices actually results from runaway Joule self-heating governed by a bulk electrical conduction mechanism in the NbO_x that is well-described by a modified three-dimensional Poole-Frenkel (3DmodPF) expression. This has important implications for improving the performance of selectors based on this principal. It provides, for example, guidance on how to lower their leakage current and tune their threshold voltage. It also provides insight into the dynamical thermal and electrical interactions between these selectors and their adjacent memory element, which strongly impact the writing and reading processes.

The standard expression for Poole-Frenkel conduction[34] assumes carriers hop in just one dimension. Hartke[35] developed a more realistic three-dimensional treatment which Young[36] modified to include the effects of traps and donors in a fashion first applied to the one dimensional expression by earlier groups.[37–39] We will use the following for the current density in NbO_x:

$$j(F,T) = \sigma F = \sigma_0(T)\left(\frac{k_B T}{\beta}\right)^2 \left\{1 + \left(\frac{\beta\sqrt{F}}{ak_B T} - 1\right) e^{\frac{\beta\sqrt{F}}{ak_B T}}\right\} + \frac{\sigma_0(T)F}{2}, \quad (1)$$

where

$$\sigma_0(T) = e\mu N_c \left(\frac{N_d}{N_t}\right)^2 e^{-\frac{E_d+E_t}{2k_B T}}.$$

Here, $\beta = \left(\frac{q^3}{\pi\varepsilon_0\epsilon_i}\right)^{\frac{1}{2}}$, F = electric field, k_B = Boltzmann's constant, μ = electron mobility, N_d and N_t are the volume densities of donors and traps, respectively, and E_d and E_t are the corresponding energies. N_c is the effective density of states in the conduction band, and ϵ_i is the high frequency dielectric constant. Equation (1) is modified from Young's by including the quantity a in the prefactor for the exponential term and by retaining terms important at low field. These corrections ensure the predicted current density goes to zero at zero field. The quantity a is unity for standard Poole-Frenkel conduction and two in the modified process. Note that in the latter case the factor β/a mimics the value of β that scales the energy barrier lowering term in the standard expression for Schottky emission.[40] This fact is often used to explain what is referred to as anomalous Poole-Frenkel conduction, i.e.,

bulk conduction that has the exponential dependence on electric field and temperature expected for interface-limited Schottky emission.

The electrical conductance described by Eq. (1) grows rapidly with increasing temperature. Consequently, as the current driven through the NbO_x increases the resulting Joule-heating induced temperature rise leads to increased conductivity and, therefore, greater power dissipation. This produces further increases in temperature. At a critical current, this positive feedback results in NDR. A simple but accurate compact model for this behavior is obtained by assuming the temperature, T_N, of the active region of the NbO_x is uniform and described by

$$C_{th}\frac{dT_N}{dt} = \frac{T_{amb} - T_N}{R_{th}} + IV. \quad (2)$$

Here, R_{th} is the effective thermal impedance between the current-carrying portion of the NbO_x and the surrounding ambient environment. Similarly, C_{th} is the effective thermal capacitance of the active region. This is illustrated by an equivalent thermal circuit in Fig. 1. In this model, the NbO_x can be viewed as a locally active memristor[41,42] with the temperature T_N as the dynamical state variable. Eqs. (1) and (2) serve, respectively, as the instantaneous conduction and dynamical state equations in this formalism. In the static limit, Eq. (2) becomes $T_N = T_{amb} + R_{th}IV$. This expression can be substituted for T in Eq. (1) to obtain a transcendental equation for the current as a function of voltage that is readily solved numerically. Alexandrov[43] used a similar quasistatic approach to describe the NDR that occurs during the electrical forming process in TiO_2 memristors, with the electrical conduction attributed to small polaron conduction for that material.

We have used Eqs. (1) and (2) to simultaneously fit sets of quasistatic V-I curves taken over a range of ambient temperatures for type I and type II formed devices with a variety of NbO_x layer thicknesses and bottom electrode diameters. Representative results for a 52 nm diameter device with an 8 nm thick NbO_x film that underwent type I forming are displayed in Figure 2(a) for temperatures between 275 and 450 K. These data were taken using an MMR Technologies Variable Temperature Microprobe System.[44] Our compact model accurately matches the data. The fitting parameters were determined by first plotting the natural logarithm of the measured low bias conductivity as a function of 1/T as indicated in Figure 2(b). The slope and intercept of this Arrhenius plot yield the energy $E \equiv (Ed + Et)/2$ and prefactor $\sigma_p \equiv e\mu N_c\left(\frac{N_d}{N_t}\right)^2$ because in the low field limit Eq. (1) implies

$$\sigma_{low}(T) = \frac{a^2+1}{2a^2}\sigma_0(T) = \sigma_p\left(\frac{a^2+1}{2a^2}\right)e^{-\frac{E}{k_BT}}.$$

In all cases, we assumed a = 2. The full V-I curves were then matched at all the measured ambient temperatures by choosing a single temperature-independent value for each of two parameters: $R_{th} = 1.27 \times 10^6$ K/W and $\epsilon_i = 22$. Similar temperature-dependent sets of V-I curves for devices with diameters between 32 and 165 and NbO_x thicknesses from 8 to 42 nm were modeled with comparably close agreement between theory and data (see supplementary Figure S2).[50] The values determined for the activation energy E ranged from 0.15 to 0.24 eV. In all cases, a value of $\epsilon_i = 22$ worked well, implying an index of refraction at frequencies near the visible of $n_i = \sqrt{\epsilon_i} \sim 4.7$. This is in reasonable agreement with ellipsometric measurements on NbO_x films with compositions close to NbO_2, which yield values for n_i between 2.3 and 2.9 at 633 nm. Note that the dielectric constant used in Eq. (1) should be specified at frequencies relevant to charge carrier motion and may differ somewhat from that observed at optical frequencies. Note, too, that if a were assumed to be 1 rather than 2 the n_i value derived from the V-I fits would be a few times higher, which is physically unrealistic and evidence that a = 2 is the correct choice for our 3DmodPF model.

To check the validity of the R_{th} values determined from fitting T-dependent V-I curves for devices with varying physical dimensions, we numerically simulated[45] our selectors using their exact geometry and literature values for their constituent materials' thermal properties. An effective R_{th} was estimated from the ratio of the average steady-state temperature gain to the heat dissipated in the active volume of the NbO_x. Both the magnitude of the simulated R_{th} values and their dependence on NbO_x thickness and device diameter agree well with the trends observed in the values obtained by fitting the V-I data for devices with 5 different geometries (Figure 3).

These results strongly support our 3DmodPF-based model for the electrical conduction in these selectors. We attempted to fit our electrothermal data to a variety of other models but none describe the conduction over the studied range of electric fields, ambient temperatures, and NbO_x layer thicknesses as accurately. In particular, the electric field dependence of other bulk conduction mechanisms, including small polaron transport and alternative hopping models, does not match the data. Interface-controlled conduction in the form of Schottky emission gives reasonable fits at higher biases but only when assuming an anomalously large ϵ_i. In the low bias ohmic regime, the conduction varies inversely with NbO_x thickness, consistent with bulk-

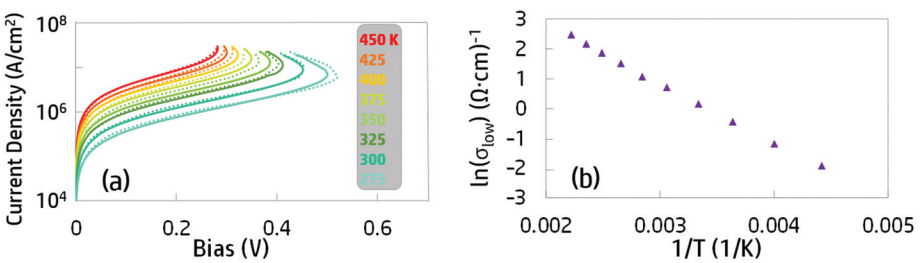

FIG. 2. (a) Measured (solid) and calculated (dashed) V-I curves for TiN/NbO_x/TiN selector with 52 nm diameter bottom electrode and 8 nm thick NbO_x layer for $T_{amb} = 275$–450 K. (b) Arrhenius plot of the conductance measured at biases low enough for it to be ohmic.

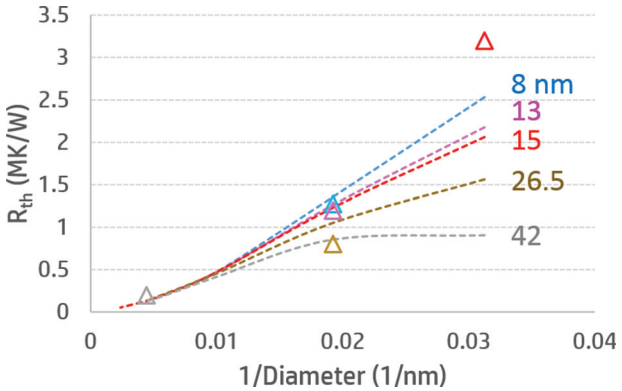

FIG. 3. Comparison of values for the thermal impedance (R_{th}) determined from fitting temperature dependent V-I data (symbols) with the predictions of a numerical simulation (dashed curves) for devices with different geometries. Simulation curves are labeled with the NbO_x layer thickness and plotted versus the inverse of the bottom electrode diameter.

dominated conduction. The Schottky emission model, however, predicts a low bias conductance independent of thickness. To verify the lack of interfacial impedance, we tested samples where the top TiN electrode was replaced with niobium nitride (NbN). The V-I curves for these devices showed no polarity dependence despite the expectation that the NbN top electrode's work function[46] is somewhat larger than that of the bottom TiN electrode,[47] although the symmetry can conceivably be explained by interfacial Fermi level pinning.

Interestingly, the correlation between the energy and the conductivity prefactor determined from the 3DmodPF fits of the V-I data is consistent with the Meyer-Neldel[48] behavior often observed in bulk transport through disordered materials at low fields. Namely, there is a relationship of the form $\sigma_p = \sigma_{00}\exp\left(\frac{E}{k_B T_{MN}}\right)$ for devices with different NbO_x thicknesses, compositions, and state of crystallization (see supplementary Figure S3).[50] The quantity T_{MN} is typically described as the isokinetic temperature for which the hopping kinetics are independent of the barrier energy E. Fits of a limited number of samples suggest that T_{MN} is $\sim$536 K for type I amorphous samples and $\sim$368 K for type II crystalline NbO_2 samples, although more samples are required to verify these numbers. Similarly, $\sigma_{00} \sim 3240$ and $\sim$245 S/m for type I and type II, respectively. The T_{MN} values are similar to those obtained for some amorphous and nanocrystalline chalcogenides.[49]

Our model guides engineering of the properties of devices that rely on Joule heating from highly non-linear conduction mechanisms to produce NDR. For selectors based on 3DmodPF conduction, it shows that the NDR onset is shifted to lower currents by increasing either the thermal isolation R_{th} or activation energy E. This is important in minimizing the leakage current through selectors used in large crossbar memory applications. Similarly, the NDR threshold voltage is increased (decreased) by increasing (decreasing) either E or the NbO_x thickness. As an example, our model predicts the leakage current through a 15 nm thick NbO_x layer, at half the NDR threshold voltage, can be decreased four fold while maintaining the same threshold voltage if R_{th} is increased by a factor of 2.5 and the NbO_x is made 10 nm thicker. Even greater reductions are possible if more oxygen rich NbO_x compositions or alternative materials with larger hopping energies can be stabilized (e.g., by using inert electrodes or a thin oxygen diffusion barrier).

In summary, we have shown that NDR observed in NbO_x is due to self-heating via a bulk conduction mechanism that is well described by three-dimensional Poole-Frenkel conduction modified by the presence of donors and traps. More generally, NDR can result from any conduction mechanism with a temperature and electric field dependence such that thermal runaway occurs at sustainable fields and temperatures. This presents additional options for creating S-type NDR devices for applications such as selectors in emerging non-volatile crossbar memory arrays. For instance, employing interface-limited conduction mechanisms such as Schottky emission allows tailoring of the characteristic activation energy, in this case the Schottky barrier height, over a broad range (see supplementary material for the equations governing NDR based on a self-heating Schottky emitter).[50] Another advantage of self-heating based NDR is that it can occur at relatively low internal temperatures. Using the fitted value of R_{th}, we estimate the temperature at the NDR onset to be 380–400 K in our NbO_x selectors, far lower than the 1080 K transition temperature of the IMT. This relatively low operating temperature affords power and durability advantages.

The authors gratefully acknowledge SK Hynix Inc. for supplying the planarized substrates containing TiN nanovias on which we built the NbO_x selectors. The authors also thank Doug Ohlberg and Bill Stickle for XPS measurements, Kate Norris and Bill Thompson for help with TEM measurements, and John Paul Strachan, Catherine Graves, Miao Hu, Xia Sheng, Steven Barcelo, Hans Cho, and Emmanuelle Merced Grafals for fruitful discussions.

[1]L. Esaki, Phys. Rev. **109**, 603 (1958).
[2]R. Tsu and L. Esaki, Appl. Phys. Lett. **22**, 562 (1973).
[3]E. F. Schubert, J. E. Cunningham, and W. T. Tsang, Appl. Phys. Lett. **51**, 817 (1987).
[4]X. Zhu, X. Zheng, M. Pak, M. O. Tanner, and K. L. Wang, Appl. Phys. Lett. **71**, 2190 (1997).
[5]S. R. Ovshinsky, Phys. Rev. Lett. **21**, 1450 (1968).
[6]D. Adler, M. S. Shur, M. Silver, and S. R. Ovshinsky, J. Appl. Phys. **51**, 3289 (1980).
[7]A. Pirovano and A. L. Lacaita, IEEE Trans. Electron Devices **51**, 452 (2004).
[8]D. Ielmini, Phys. Rev. B **78**, 035308 (2008).
[9]L. O. Chua, J. Yu, and Y. Yu, IEEE Trans. Circuits Syst. **32**, 46 (1985).
[10]H. Futaki, Jpn. J. Appl. Phys., Part 1 **4**, 28 (1965).
[11]R. G. Cope and A. W. Penn, J. Phys. D: Appl. Phys. **1**, 161 (1968).
[12]C. N. Berglund, IEEE Trans. Electron Devices **16**, 432 (1969).
[13]J. Duchene, M. Terraillon, P. Pailly, and G. Adam, Appl. Phys. Lett. **19**, 115 (1971).
[14]H. T. Kim, B. J. Kim, S. Choi, B. G. Chae, Y. W. Lee, T. Driscoll, M. M. Qazilbash, and D. N. Basov, J. Appl. Phys. **107**, 023702 (2010).
[15]K. L. Chopra, Proc. IEEE **51**, 941 (1963).
[16]K. L. Chopra, J. Appl. Phys. **36**, 184 (1965).
[17]F. Argall, Solid-State Electron. **11**, 535 (1968).
[18]R. J. Soukup, J. Appl. Phys. **43**, 3431 (1972).
[19]G. Taylor and B. Lalevic, J. Appl. Phys. **48**, 4410 (1977).
[20]R. C. Morris, J. E. Christopher, and R. V. Coleman, Phys. Rev. **184**, 565 (1969).
[21]D. S. Jeong, H. Schroeder, and R. Waser, Electrochem. Solid-State Lett. **10**, G51 (2007).
[22]L. Goux, J. G. Lisoni, M. Jurczak, D. J. Wouters, L. Courtade, and Ch. Muller, J. Appl. Phys. **107**, 024512 (2010).

[23]M. D. Pickett, J. Borghetti, J. Joshua Yang, G. Medeiros-Ribeiro, and R. S. Williams, Adv. Mater. **23**, 1730 (2011).
[24]Y. Fujisaki, Jpn. J. Appl. Phys., Part 1 **52**, 040001 (2013).
[25]G. W. Burr, R. S. Shenoy, K. Virwani, P. Narayanan, A. Padilla, and B. Kurdi, J. Vac. Sci. Technol., B **32**, 040802 (2014).
[26]G. A. Gibson, "General Conditions for Occurrence of Self-Heating Enabled Negative Differential Resistance" (to be published).
[27]F. A. Chudnovskii, L. L. Odynets, A. L. Pergaments, and G. B. Stefanovich, J. Solid State Chem. **122**, 95 (1996).
[28]X. Liu, S. Ma. Sadaf, M. Son, J. Park, J. Shin, W. Lee, K. Seo, D. Lee, and H. Hwang, IEEE Electron Device Lett. **33**, 236 (2012).
[29]M. D. Pickett and R. S. Williams, Nanotechnology **23**, 215202 (2012).
[30]X. Liu, S. K. Nandi, D. K. Venkatachalam, K. Belay, S. Song, and R. G. Elliman, IEEE Electron Device Lett. **35**, 1055 (2014).
[31]M. Kang, S. Yu, and J. Son, J. Phys. D: Appl. Phys. **48**, 095301 (2015).
[32]S. K. Nandi, X. Liu, D. K. Venkatachalam, and R. G. Elliman, J. Phys. D: Appl. Phys. **48**, 195105 (2015).
[33]R. F. Jannick, J. Phys. Chem. Solids **27**, 1183 (1966).
[34]J. Frenkel, Tech. Phys. USSR **5**, 685 (1938); Phys. Rev. **54**, 647 (1938).
[35]J. L. Hartke, J. Appl. Phys. **39**, 4871 (1968).
[36]P. L. Young, J. Appl. Phys. **47**, 235 (1976).
[37]J. R. Yeargan and H. L. Taylor, J. Appl. Phys. **39**, 5600 (1968).
[38]P. Mark and T. E. Hartman, J. Appl. Phys. **39**, 2163 (1968).
[39]J. G. Simmons, Phys. Rev. **155**, 657 (1967).
[40]P. R. Emtage and W. Tantraporn, Phys. Rev. Lett. **8**, 267 (1962).
[41]L. Chua and S. Kang, Proc. IEEE **64**, 209 (1976).
[42]A. Ascoli, S. Slesazeck, H. Mähne, R. Tetzlaff, and T. Mikolajick, IEEE Trans. Circuits Syst. **62**, 1165 (2015).
[43]A. S. Alexandrov, A. M. Bratkovsky, B. Bridle, S. E. Savel'ev, and D. B. Strukov, Appl. Phys. Lett. **99**, 202104 (2011).
[44]See http://www.mmr-tech.com for MMR Technologies.
[45]See http://www.comsol.com for Comsol Multiphysics.
[46]N. van Hoornick, H. De Witte, T. Witters, C. Zhao, T. Conard, H. Huotari, J. Swerts, T. Schram, J. W. Maes, S. De Gendt, and M. Heyns, J. Electrochem. Soc. **153**, G437 (2006).
[47]L. Bolotov, K. Fukuda, T. Tada, T. Matsukawa, and M. Masahara, Jpn. J. Appl. Phys., Part 1 **54**, 04DA03 (2015).
[48]W. Meyer and H. Neldel, Z. Tech. Phys. **12**, 588 (1937).
[49]F. Abdel-Wahab and A. Yelon, J. Appl. Phys. **114**, 023707 (2013).
[50]See supplementary material at http://dx.doi.org/10.1063/1.4939913 for additional figures and discussion.